BIOLOGICAL CRYSTALLOGRAPHY

ISSN 1399-0047

Structures of complexes of type 5 17β-hydroxysteroid dehydrogenase with structurally diverse inhibitors: insights into the conformational changes upon inhibitor binding

Yasushi Amano,* Tomohiko Yamaguchi, Tatsuya Niimi and Hitoshi Sakashita

Drug Discovery Research, Astellas Pharma Inc., 21 Miyukigaoka, Tsukuba, Ibaraki 305-8585, Japan. *Correspondence e-mail: yasushi-amano@astellas.com

Received 10 September 2014
Accepted 2 February 2015

Edited by S. Wakatsuki, Stanford University, USA

Keywords: type 5 17β-hydroxysteroid dehydrogenase; prostate cancer.

PDB references: 17β-HSD5, complex with compound **1**, 4xve; complex with compound **2**, 4wdt; complex with compound **3**, 4wdu; complex with compound **4**, 4xvd; complex with compound **5**, 4wdw; complex with compound **6**, 4wdx

Supporting information: this article has supporting information at journals.iucr.org/d

Type 5 17β-hydroxysteroid dehydrogenase (17β-HSD5) is an aldo-keto reductase expressed in the human prostate which catalyzes the conversion of androstenedione to testosterone. Testosterone is converted to 5α-dihydrotestosterone, which is present at high concentrations in patients with castration-resistant prostate cancer (CRPC). Inhibition of 17β-HSD5 is therefore considered to be a promising therapy for treating CRPC. In the present study, crystal structures of complexes of 17β-HSD5 with structurally diverse inhibitors derived from high-throughput screening were determined. In the structures of the complexes, various functional groups, including amide, nitro, pyrazole and hydroxyl groups, form hydrogen bonds to the catalytic residues His117 and Tyr55. In addition, major conformational changes of 17β-HSD5 were observed following the binding of the structurally diverse inhibitors. These results demonstrate interactions between 17β-HSD5 and inhibitors at the atomic level and enable structure-based drug design for anti-CRPC therapy.

1. Introduction

Type 5 17β-hydroxysteroid dehydrogenase (17β-HSD5), also known as AKR1C3, belongs to the AKR1C subfamily, the members of which catalyze the reduction of ketosteroids and ketoprostaglandins (Byrns *et al.*, 2011). 17β-HSD5 is expressed in the human prostate and catalyzes the conversion of androstenedione to testosterone (Penning *et al.*, 2000). Testosterone is converted to 5α-dihydrotestosterone (DHT), which is present at high concentrations in patients with castration-resistant prostate cancer (CRPC; Labrie, 2011). Inhibition of 17β-HSD5 is therefore a promising therapy for CRPC.

At present, there are 30 crystal structures of 17β-HSD5 in the Protein Data Bank (Lovering *et al.*, 2004; Komoto *et al.*, 2004, 2006; Qiu *et al.*, 2004, 2007; Chen *et al.*, 2012; Liedtke *et al.*, 2013; Jamieson *et al.*, 2012; Heinrich *et al.*, 2013; Flanagan *et al.*, 2012, 2014; Jackson *et al.*, 2012). Lovering and coworkers reported the first crystal structure of 17β-HSD5 (Lovering *et al.*, 2004). As expected from sequence alignment, 17β-HSD5 forms a typical aldo-keto reductase structure, and its catalytic pocket is mainly formed by loops A (116–143), B (217–238) and C (298–323) (Fig. 1). As previously reported (Byrns *et al.*, 2011), the ligand-binding pocket of 17β-HSD5 can be divided into five compartments as follows: an oxyanion site, a steroid channel and subpockets SP1, SP2 and SP3 (Fig. 2). The oxyanion site consists of the cofactor NADP$^+$ and the catalytic residues Tyr55 and His117, which are conserved among AKR1C enzymes. The steroid channel is formed by Tyr24, Leu54, Ser129 and Trp227 and is open to solvent, guiding

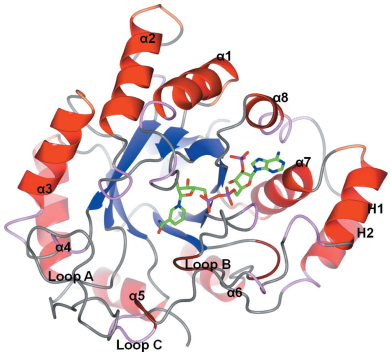

substrates into the oxyanion site. The SP1 pocket is located inside the ligand-binding pocket and is surrounded by Ser118, Asn167, Phe306, Phe311 and Tyr319. In contrast, the SP2 pocket is located in a shallow region surrounded by Trp86, Leu122, Ser129 and Phe311, while the SP3 pocket is located near the phosphate moiety of $NADP^+$ and is surrounded by Tyr24, Glu192, Ser221 and Tyr305.

The majority of 17β-HSD5 inhibitors were developed based on nonsteroidal anti-inflammatory drugs (NSAIDs) such as flufenamic acid and indomethacin (Adeniji *et al.*, 2013). These inhibitors contain a carboxylate group that binds to the oxyanion site and forms strong hydrogen bonds to Tyr55 and His117 (Lovering *et al.*, 2004; Chen *et al.*, 2012). However, while the carboxylate group contributes to potent inhibitory activity, it might also affect the transport of 17β-HSD5 inhibitors into cells. Recently, several noncarboxylate inhibitors have been identified. Heinrich and coworkers reported the discovery of a new class of pyrrolidinone inhibitors generated by conversion of the carboxylate to a pyrrolidinone. Interestingly, despite their potent inhibitory activity, crystallographic studies revealed that the pyrrolidinone does not form direct hydrogen bonds to Tyr55 or His117 (Heinrich *et al.*, 2013). The same group next identified a morpholylurea as a potent 17β-HSD5 inhibitor *via* high-throughput screening (HTS). Crystallographic study of the morpholylurea inhibitor revealed that the carbonyl O atom of the urea moiety bound to the oxyanion site and formed a hydrogen bond to Tyr55 (Flanagan *et al.*, 2014).

Astellas Pharma conducted HTS using a 17β-HSD5 enzyme assay against an in-house chemical library and synthesized potent noncarboxylate inhibitors of 17β-HSD5 (Watanabe *et al.*, 2013). Although the details have not been reported, structurally diverse inhibitors, including noncarboxylate compounds, were identified from HTS. To identify interactions between the inhibitors and protein, particularly the oxyanion site, we analyzed the crystal structures of 17β-HSD5 in complex with compounds from HTS and the potent compounds that were optimized by Watanabe and coworkers. We discuss the results of our crystallographic studies and conformational changes upon inhibitor binding.

2. Materials and methods

2.1. Expression and purification of 17β-HSD5

Recombinant 17β-HSD5 was designed, expressed and purified based on previously reported methods (Lovering *et al.*, 2004). Full-length cDNA of human 17β-HSD5 (GenBank accession No. NM_003739) was subcloned into a pET-22 vector (Merck Millipore KGaA, Darmstadt, Germany) containing a C-terminal His_6 tag and used to transform *Escherichia coli* BL21(DE3) cells (Merck Millipore). Cells were grown in Terrific Broth medium (20 g yeast extract, 10 g polypeptone, 4.33 g disodium hydrogen phosphate, 2.65 g potassium dihydrogen phosphate and 4 ml glycerol per litre) at 37°C to an OD_{600} of 3–4. Following reduction of the temperature to 15°C, isopropyl β-D-thiogalactoside was added to a final concentration of 1 m*M* and the cells were grown for an additional 44 h. The cells were harvested by centrifugation and stored at −80°C. Frozen cell pellets were suspended in lysis buffer [500 m*M* potassium phosphate pH 8.0, 1 m*M* phenylmethylsulfonyl fluoride, 0.1%(*v*/*v*) β-mercaptoethanol, 0.2 mg ml^{-1} lysozyme].

The cells were disrupted by sonication and debris was removed by centrifugation. Polyethyleneimine was added to a final concentration of 0.05%(*v*/*v*) and precipitate was removed by centrifugation. After centrifugation, the supernatant was

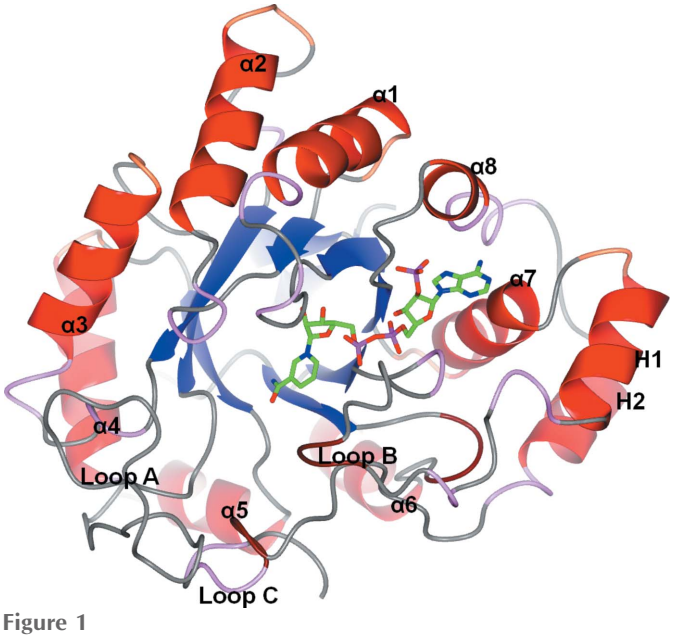

Figure 1
Ribbon diagram of the overall structure of 17β-HSD5 (PDB entry 1s1p). The green stick model indicates $NADP^+$.

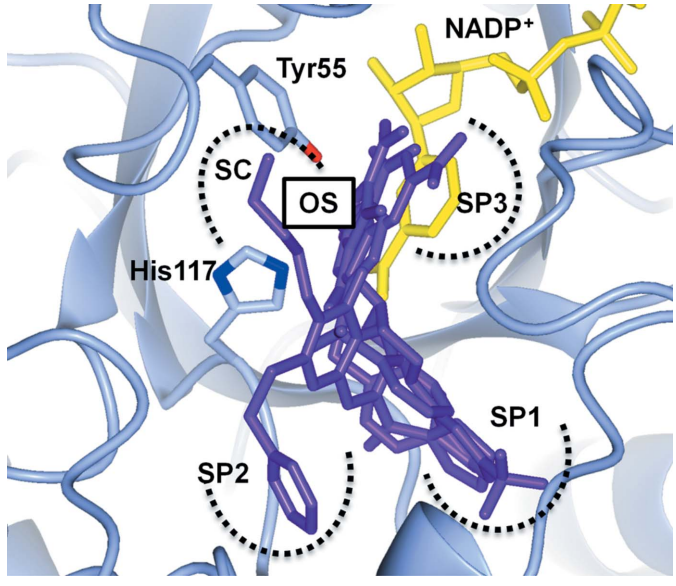

Figure 2
Superimposition of compounds **1**–**4** in 17β-HSD5 ternary-complex structures. Purple stick models indicate compounds **1**–**4**. Yellow stick models indicate $NADP^+$. Dashed lines indicate the oxyanion site (OC), subpockets 1–3 (SP1–SP3) and the steroid channel (SC).

adjusted to 60% saturated ammonium sulfate. The suspension was centrifuged and the precipitate was suspended in buffer *A* [10 m*M* potassium phosphate pH 7.4, 300 m*M* NaCl, 10%(*v*/*v*) glycerol, 20 m*M* imidazole] and then loaded onto an Ni–NTA Superflow column (Qiagen, Valencia, California, USA) equilibrated with buffer *A*. The column was washed with buffer *A* and the protein was eluted by increasing the imidazole concentration to 250 m*M*. The eluate was diluted twice with buffer *A* without NaCl or imidazole. The diluted eluate was then loaded onto a Q-Sepharose Fast Flow ion-exchange column (GE Healthcare, Buckinghamshire, England) and eluted with a step gradient of NaCl. The fractions containing 17β-HSD5 were collected and further purified using a HiLoad 16/60 Superdex 200 size-exclusion column (GE Healthcare) using buffer *B* (10 m*M* potassium phosphate pH 7.4, 500 m*M* NaCl, 1 m*M* ethylenediaminetetraacetic acid, 1 m*M* dithiothreitol) as an eluent. Although we did not check the specific activity of the purified protein, it was expected to have a similar activity to the previously reported recombinant protein (Lovering *et al.*, 2004) because there were no major differences in the procedure. For crystallization, NaCl was removed by repeated ultrafiltration using Amicon Ultra-15 (10 000 MWCO, Merck Millipore), concentrated to 15 mg ml^{-1} and stored at 4°C.

2.2. Crystallization, data collection and refinement

Crystals were grown by the sitting-drop vapour-diffusion method. Cocrystals of 17β-HSD5 and compounds **1**–**4** (Fig. 3) were obtained by cocrystallization with a fivefold molar excess of NADP$^+$ and a threefold molar excess of each inhibitor. Crystals were grown in 0.1 *M* sodium citrate pH 5.5, 0.4 *M* ammonium acetate, 2.5%(*v*/*v*) 2-methyl-2,4-pentanediol, 22–30%(*w*/*v*) PEG 4000. Crystals of 17β-HSD5 in complex with compounds **5** or **6** were obtained *via* cocrystallization with a threefold molar excess of each inhibitor and were grown in 0.1 *M* HEPES pH 6.5, 0.2 *M* ammonium dihydrogen phosphate, 20–25%(*w*/*v*) PEG 3350. Diffraction data for complexes of 17β-HSD5 with compounds **1**–**4** were collected on the AR-NW12A beamline at the Photon Factory, KEK (Chavas *et al.*, 2012). Diffraction data for 17β-HSD5 with compounds **5** and **6** were collected on a Rigaku FR-E+ SuperBright rotating-anode X-ray generator equipped with a Rigaku R-AXIS VII area detector. Data were processed and scaled using *HKL-2000* (Otwinowski & Minor, 1997). Structures were solved by molecular replacement with *MOLREP* (Vagin & Teplyakov, 2010) using the previously reported 17β-HSD5 structure with NADP$^+$ (PDB entry 1s1p; Lovering *et al.*, 2004). After initial refinement with *REFMAC* (Murshudov *et al.*, 2011), inhibitors were fitted to clearly observed electron densities and library descriptions were generated using *AFITT* (OpenEye Scientific). Ternary models were manually constructed using *Coot* (Emsley & Cowtan, 2004) and refined using *REFMAC*. The solvent was modelled and refined, and statistics are shown in Table 1.

2.3. Enzyme assay

17β-HSD5 inhibition assays were conducted as described previously (Watanabe *et al.*, 2013). Briefly, 9,10-phenanthrenequinone (9,10-PQ) was used as the substrate and the oxidation of the cofactor NADPH was measured by monitoring the change in absorbance at 340 nm. Purified enzyme (at a final concentration of 10 µg ml^{-1}), 9,10-PQ (4 µmol l^{-1}), NADPH

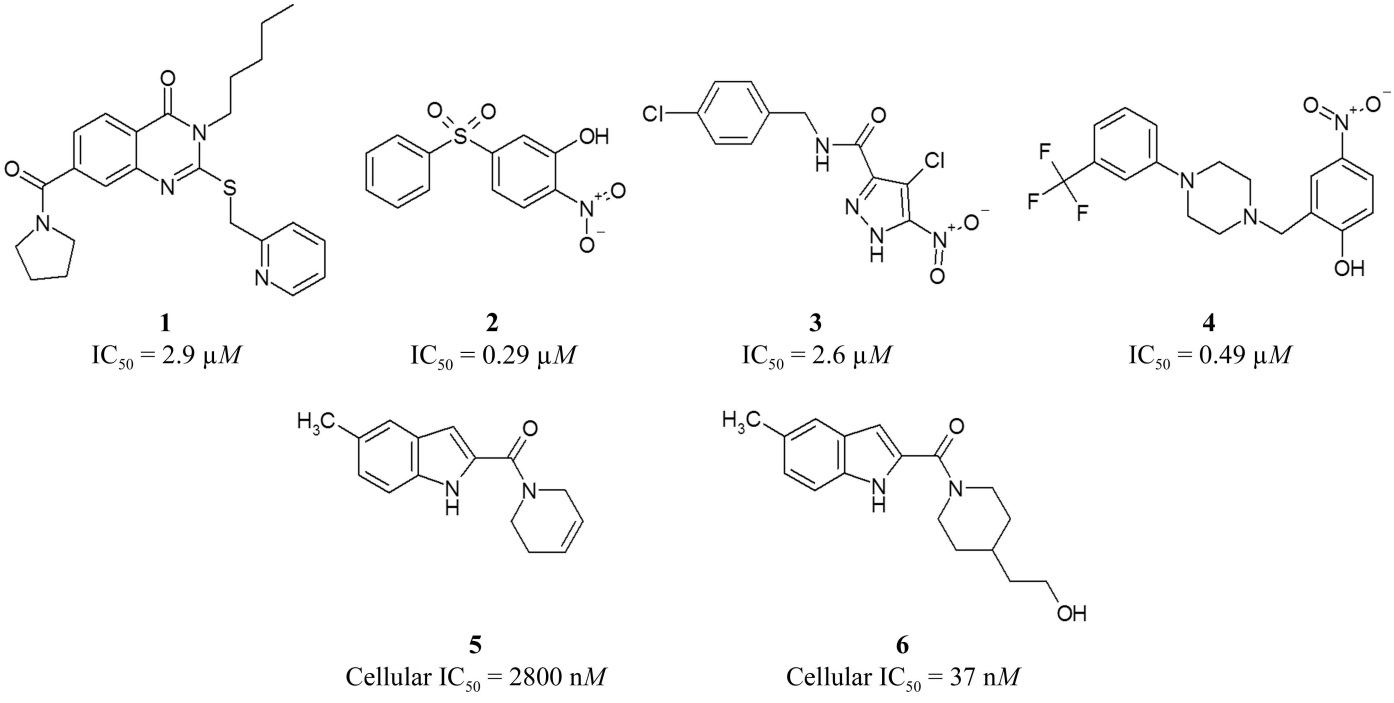

Figure 3
Chemical structures of compounds **1**–**6**. The IC_{50} values of compounds **1**–**4** are based on 17β-HSD5 enzyme assays. The cellular IC_{50} values of compounds **5** and **6** have previously been reported (Watanabe *et al.*, 2013).

Table 1
Data-processing and refinement statistics.

Values in parentheses are for the outer shell.

Compound	**1**	**2**	**3**	**4**	**5**	**6**
PDB entry	4xve	4wdt	4wdu	4xvd	4wdw	4wdx
Space group	$P2_12_12_1$	$P2_12_12_1$	$P2_12_12_1$	$I4$	$P1$	$P2_1$
Unit-cell parameters						
a (Å)	55.3	55.5	55.4	145.8	55.1	60.0
b (Å)	62.6	62.6	62.3	145.8	57.9	77.2
c (Å)	95.7	96.2	96.0	74.3	60.3	72.2
α (°)	90	90	90	90	81.0	90
β (°)	90	90	90	90	69.7	97.6
γ (°)	90	90	90	90	79.1	90
Resolution (Å)	41.4–1.55 (1.59–1.55)	38.1–1.50 (1.54–1.50)	38.0–1.70 (1.74–1.70)	40.7–2.81 (2.89–2.81)	14.6–1.94 (1.99–1.94)	14.3–1.64 (1.68–1.64)
Multiplicity	3.5 (3.1)	3.9 (3.8)	4.3 (4.1)	3.2 (3.1)	1.9 (1.8)	3.6 (3.3)
Average $I/\sigma(I)$	16.0 (2.1)	18.7 (2.8)	17.3 (2.4)	11.0 (2.6)	6.9 (1.8)	6.7 (1.3)
$R_{\rm merge}$† (%)	10.1 (45.4)	8.1 (39.3)	9.4 (46.2)	10.1 (45.4)	6.0 (23.4)	6.0 (41.5)
No. of reflections	46111 (3277)	47351 (3393)	29604 (2282)	16372 (1202)	44978 (3159)	72670 (5139)
Completeness (%)	99.4 (97.4)	91.5 (91.8)	83.4 (88.0)	90.4 (91.2)	93.6 (91.3)	95.7 (93.2)
$R_{\rm work}$‡ (%)	18.0	17.8	19.9	20.9	20.2	21.6
$R_{\rm free}$‡ (%)	20.3	20.4	23.1	25.9	25.3	24.9
Average B factor (Å^2)	14.9	12.9	15.9	33.6	30.5	27.6
R.m.s.d., bond lengths (Å)	0.026	0.026	0.021	0.012	0.019	0.022
R.m.s.d., bond angles (°)	2.575	2.532	2.186	1.628	2.131	2.253
Ramachandran plot (%)						
Preferred	96.5	96.8	97.1	96.1	95.9	96.9
Allowed	2.6	2.2	1.9	3.6	2.9	2.7
Outliers	1.0	1.0	1.0	0.4	1.2	0.3

† $R_{\rm merge} = \sum_{hkl}\sum_i |I_i(hkl) - \langle I(hkl)\rangle| / \sum_{hkl}\sum_i I_i(hkl)$, where $I_i(hkl)$ is the intensity of an individual reflection and $\langle I(hkl)\rangle$ is the mean intensity obtained from multiple observations of symmetry-related reflections. ‡ $R_{\rm work} = \sum_{hkl} ||F_{\rm obs}| - |F_{\rm calc}|| / \sum_{hkl} |F_{\rm obs}|$. A randomly omitted 5% of the reflections were used to calculate $R_{\rm free}$.

(200 µmol l^{-1}) and the test compound were mixed in 100 m*M* potassium phosphate buffer pH 6.0. After incubation for 10–20 min at room temperature, the absorbance at 340 nm was measured using a SAFIRE spectrophotometer (Tecan). A dose–response curve was plotted and the IC_{50} was calculated. As reported by Byrns *et al.* (2008), enzyme assays using 9,10-PQ as the substrate are likely to evaluate uncompetitive inhibitory activity of the compounds.

3. Results and discussion

3.1. Crystal structure of 17β-HSD5 complexed with compound 1 and NADP$^+$

The crystal structure of 17β-HSD5 complexed with compound **1** was determined at 1.55 Å resolution (*R* factor = 18.1%, $R_{\rm free}$ = 20.2%). The crystal belonged to space group $P2_12_12_1$ and has similar unit-cell parameters to those of PDB entry 1s1p (crystal form I). Compound **1** binds to the SP1, SP2 and SP3 pockets (Fig. 4*a*). Interestingly, compound 1 does not form hydrogen bonds to Tyr55 or His117. Instead, an ambiguous electron-density map was observed in the oxyanion site (Fig. 5*a*). Although we could not specify what molecule bound in the oxyanion site, it does not seem to affect the binding mode of compound **1**. Compound **1** forms two hydrogen bonds to 17β-HSD5 or a water molecule. The O atom of the amide moiety forms a hydrogen bond to the side chain of Ser118 (2.65 Å). The N atom of the pyridine ring forms a hydrogen bond to Ser87 *via* a water molecule. The bridge S atom makes a sulfur–oxygen interaction with Ser129. The pyrrolidine moiety binds to the SP1 pocket, the pyridine moiety to the SP2 pocket and the pentyl moiety to the steroid channel. Although the overall structure of compound **1** bound to 17β-HSD5 is similar to that of PDB entry 1s1p (r.m.s.d. of 0.55 Å), loop A moves towards the solvent and the conformation of Phe311 is modified (Fig. 6*a*). This is triggered by insertion of the pyridine ring between the side chain of Val137 in loop A and that of Phe311 in loop C. In PDB entry 1s1p, loops A and C interact with each other *via* a hydrogen bond between the backbone NH of Val137 and the backbone O atom of Ser310. The insertion of the pyridine ring directly disrupts this interaction, and loop A is released from the core of the protein. The movement of loop A extends the SP2 pocket and forms a tunnel extending to the solvent region. Inhibitors that bind deep into the SP2 pocket might also disrupt the interaction between loops A and C, and their affinity may be increased by modifications that enable insertion into the newly formed tunnel.

3.2. Crystal structure of 17β-HSD5 complexed with compound 2 and NADP$^+$

The crystal structure of 17β-HSD5 complexed with compound **2** was determined at 1.5 Å resolution (*R* factor = 17.8%, $R_{\rm free}$ = 20.4%). The crystal belonged to crystal form I. Compound **2** binds to the oxyanion site and the SP1 pocket (Fig. 4*b*), and the hydroxyl group forms hydrogen bonds to Tyr55 (2.83 Å) and His117 (2.68 Å). The nitro group also forms a hydrogen bond to Tyr55 and a water molecule in the cluster of water molecules in the SP3 pocket. This is the first example of hydrogen bonding to the catalytic residues of 17β-HSD5 by a combination of hydroxyl and nitro groups.

Although the sulfone linker does not make specific interactions, it helps to maintain the linker at an acute angle (105.2°). This angle enables binding of the benzene ring to the SP1 pocket. The C atom at the *para* position of the benzene ring is over 5 Å away from the side chain of Tyr319, which is located at the bottom of the SP2 pocket. A substituent at the *para* position can therefore occupy the SP1 pocket and increase the inhibitory activity. The overall structure is closely similar to PDB entry 1s1p (r.m.s.d. of 0.15 Å) and the interaction between loops A and C is conserved. These findings are consistent with compound **2** binding deeply into the catalytic pocket and not penetrating the SP2 pocket.

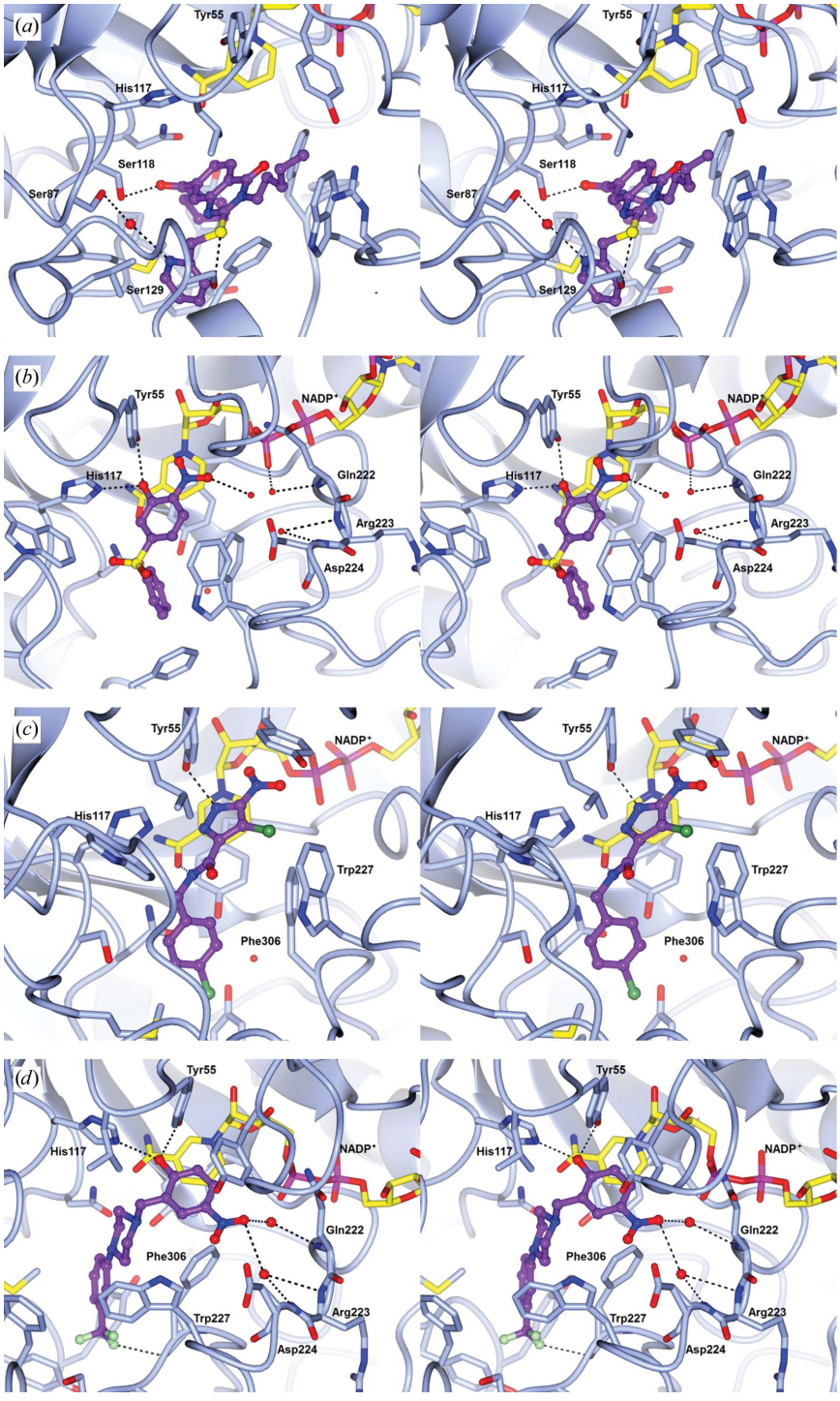

Figure 4
Stereo representations of the crystal structures of inhibitor-bound 17β-HSD5. Purple ball-and-stick models indicate compounds **1** (*a*), **2** (*b*), **3** (*c*) and **4** (*d*). Yellow stick models indicate NADP$^+$. Red balls indicate water molecules. Dashed lines indicate hydrogen bonds between the inhibitor and 17β-HSD5.

3.3. Crystal structure of 17β-HSD5 complexed with compound 3 and NADP$^+$

The crystal structure of 17β-HSD5 complexed with compound **3** was determined at 1.7 Å resolution (R factor = 19.9%, $R_{\rm free}$ = 23.1%). The crystal belonged to crystal form I. Although the completeness of the data set is 83.4% (88.0% in the outer shell; Table 1), an electron-density map for compound **3** was clearly observed. The reason for the low completeness is unclear. Compound **3** binds to the oxyanion site and the SP1 pocket (Fig. 4*c*). Interestingly, two N atoms of the pyrazole ring form hydrogen bonds to Tyr55 (2.81 Å) and His117 (2.88 Å). To our knowledge, this is the first example of a hydrogen bond between an N atom and the catalytic residues of 17β-HSD5. A possible hydrogen-bonding pattern is Tyr55 acting as a hydrogen-bond donor and His117 as a hydrogen-bond acceptor or *vice versa*. In addition, the NH of the amide forms a hydrogen bond to the nicotinamide of NADP$^+$. The *p*-chlorophenyl group binds deeply into the SP1 pocket. The chlorine substituent on the pyrazole ring forms a van der Waals interaction with Trp227 and Phe306. The overall structure is similar to PDB entry 1s1p (r.m.s.d. of 0.26 Å) and the positions and orientation of the amino-acid residues in the catalytic pocket are closely similar to those in PDB entry 1s1p. Loops A and C interact with each other as in PDB entry 1s1p or in the compound **2**-bound structure. This is consistent with compound **3** not binding to the SP2 pocket and not interfering with interaction between loops A and C.

3.4. Crystal structure of 17β-HSD5 complexed with compound 4 and NADP$^+$

Cocrystallization of compound **4** and 17β-HSD5 produced a new crystal form belonging to space group $I4$ (crystal form II). The crystal structure of compound **4** bound to 17β-HSD5 was determined at 2.81 Å resolution (R factor = 19.7%, $R_{\rm free}$ = 26.5%). The asymmetric unit of this crystal contains two molecules of 17β-HSD5

(chains *A* and *B*) with compound **4** and NADP$^+$ bound to each chain. Given that the binding mode of compound **4** and the conformation of the protein are conserved between the chains (r.m.s.d. of 0.44 Å), we describe the structure of chain *A* and that of compound **4** bound to chain *A*. Compound **4** binds to the oxyanion site, the SP1 pocket and the shallow SP3 pocket (Fig. 4*d*). The hydroxyl group of the *p*-nitrophenol moiety forms hydrogen bonds to Tyr55 (2.41 Å) and His117 (2.72 Å). The nitro group of the *p*-nitrophenol moiety interacts with the phosphate moiety of NADP$^+$ and the main-chain NH of Gln222, Arg223 and Asp224 *via* water molecules. The trifluoromethylphenyl moiety binds deeply into the SP1 pocket. The overall structure is similar to PDB entry 1s1p (r.m.s.d. of 0.80 Å), but the conformation of loop C is different, including its main-chain atoms (Fig. 6*b*). This conformational change is likely to occur *via* binding of the trifluoromethyl group to the SP1 pocket. Interaction between loop A and C is disrupted by the conformational change of both as they are moved towards the solvent. Further, the side chain of Trp227 is flipped by the binding of the nitro group of compound **4** to the SP3 pocket and van der Waals interaction with the piperazine moiety of compound **4**. Conformational change of loop C is connected to the flipping of Trp227, as the side chain of the flipped Trp227 interferes with the original position (in PDB entry 1s1p) of Phe311 in loop C. Regarding compound **4** bound to 17β-HSD5, the side chain of Phe311 is flipped and moved towards the outside of the pocket owing to the flipping of Trp227. Although the SP1 and SP3 pockets are located at either side of the catalytic pocket of 17β-HSD5 and appear to be independent of each other, our findings suggest that their structures influence each other.

3.5. Crystal structure of 17β-HSD5 complexed with compound 5 and NADP$^+$

Compound **5** was identified by Astellas Pharma (Watanabe *et al.*, 2013). After HTS, compound **5** was focused on owing to its unique chemical structure among 17β-HSD5 inhibitors. The inhibitory activity of compound **5** against 17β-HSD5 exhibited an IC_{50} value of 2800 n*M* in the cell assay. To reveal the binding modes of compound **5** and to facilitate structure-based drug design, we attempted to determine the crystal structure of 17β-HSD5 complexed with compound **5**. Firstly, cocrystallization was performed based on the crystallization conditions of previously reported 17β-HSD5 crystals, but no crystals were formed. Compound **5** was then soaked into an acetate-bound crystal (crystal form I). A range of conditions were tested, including long periods of time, high concentrations of compound and different pH values and compositions of the mother liquor. However, electron density corresponding to compound **5** was not observed in the structure obtained using soaked crystals. Finally, we explored new crystallization conditions using in-house-developed screening kits, which resulted in the formation of crystals with a different appearance to those of crystal forms I or II. X-ray diffraction data were collected from this new crystal form and the structure was solved, in which electron density for compound **5** was clearly observed. The crystal belonged to space group *P*1 (crystal form III). The crystal structure of compound **5** bound to 17β-HSD5

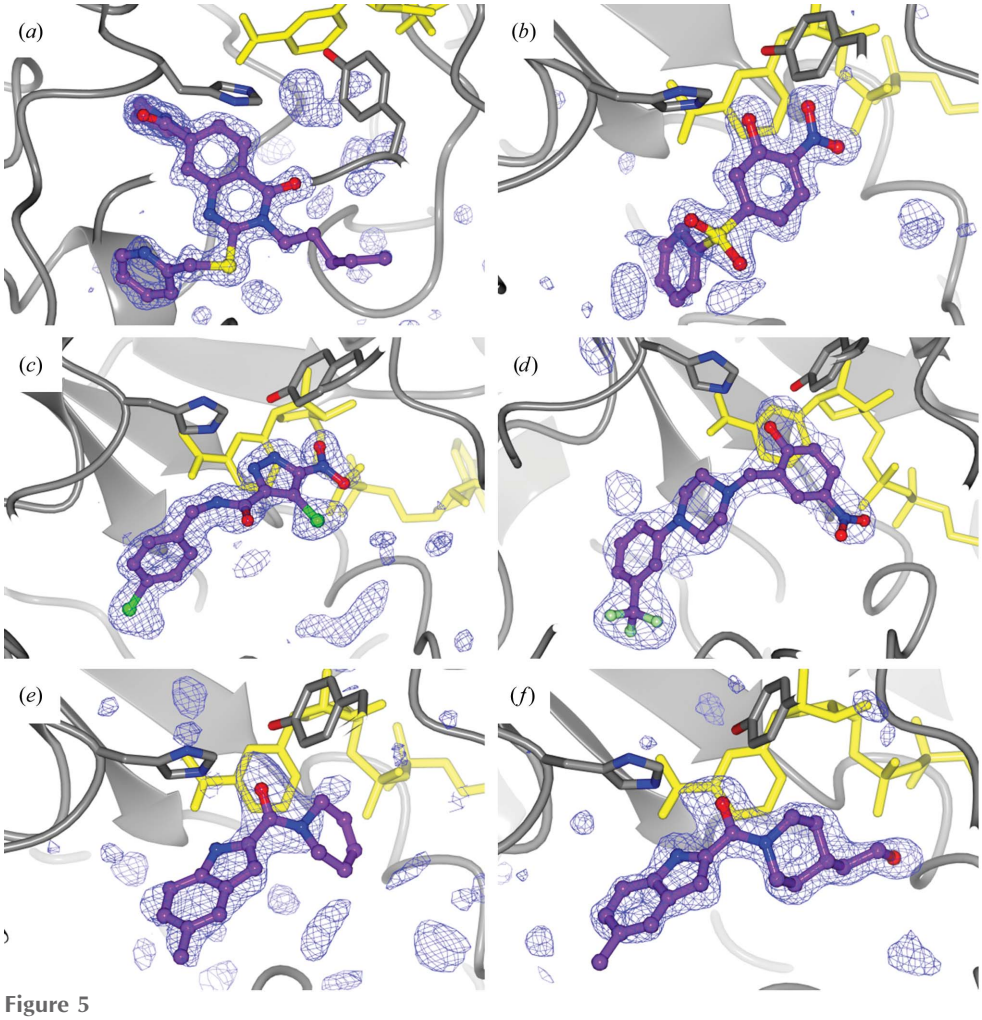

Figure 5
Electron-density maps of the inhibitors in the 17β-HSD5 catalytic pocket: (*a*) compound **1**, (*b*) compound **2**, (*c*) compound **3**, (*d*) compound **4**, (*e*) compound **5** and (*f*) compound **6**. OMIT $F_o - F_c$ maps are shown [contoured at (*a*) 3.0σ, (*b*) 3.0σ, (*c*) 2.5σ, (*d*) 2.0σ, (*e*) 2.0σ and (*f*) 2.0σ]. Purple ball-and-stick models indicate the inhibitors. Yellow thin-stick models indicate NADP$^+$. Grey ribbon diagrams indicate the protein structures.

was determined at 1.94 Å resolution (R factor = 20.1%, R_{free} = 25.3%). Two 17β-HSD5 chains (chains A and B) and two molecules of compound **5** are present in the asymmetric unit. The structures of chains A and B are similar (r.m.s.d. of 0.42 Å), and the binding mode of compound **5** is conserved between the two chains of 17β-HSD5. However, Phe306 in chain B is more clearly observed than that in chain A. In addition, Asn307 and Ser308, which are disordered in chain A, are observed in chain B. We therefore discuss the structure of chain B with a molecule of compound **5** bound to chain B. The carbonyl O atom of compound **5** forms hydrogen bonds to Tyr55 (2.65 Å) and His117 (2.91 Å) (Fig. 7*a*). The N atom of the indole ring forms a hydrogen bond to the nicotinamide of $NADP^+$ (2.69 Å). Surprisingly, the residues from Asp309 to the C-terminal end are completely disordered and the SP2 pocket is therefore not formed in this structure. The loss of the SP2 pocket is triggered by the binding of the dihydropyridine moiety at the entrance to the SP3 pocket. To admit the dihydropyridine moiety, the side chains of Trp227 in loop B and Phe306 are flipped and the positions of their C^α atoms are changed (Fig. 8). The movement of Phe306 also changes the position of the adjacent Asn307 residue.

In contrast, in PDB entry 1s1p loops B and C interact with each other *via* a hydrogen bond between the main-chain O atom of Trp227 and the main-chain NH of Asn307. Therefore, the movement of Trp227 and Phe306 disrupts this interaction and loosens the structure of loop C. Furthermore, the phenyl ring of Phe306 forms a van der Waals interaction and a weak CH–π interaction with the indole ring of compound **5**. The indole ring of compound **5** also interacts with the indole ring of Trp86, which is positioned at the opposite side of Phe306. This sandwich-like interaction may stabilize the conformation of Phe306 and help to loosen the structure of loop C. In addition, loop A also moves towards the solvent owing to a loss of interaction with loop C. We concluded that this newly found conformation of 17β-HSD5 is not artificial in the crystal because (i) the crystal is only obtained in the presence of compound **5** and (ii) neither an additional 17β-HSD5 chain in the asymmetric unit nor symmetry-related molecules affect the structure of loops A, B or C.

3.6. Crystal structure of 17β-HSD5 complexed with compound 6 and $NADP^+$

Compound **6** was generated by introducing a hydroxyethyl group into compound **5** (Watanabe *et al.*, 2013). Compound **6** exhibited potent inhibitory activity against 17β-HSD5, with an IC_{50} value of 37 nM, which is 75-fold higher than that of compound **5**. To determine the reason for this increase in inhibitory activity, we investigated the crystal structure of 17β-HSD5 complexed with compound **6**. Cocrystallization was performed based on the crystallization conditions for 17β-HSD5 complexed with compound **5** and a high-quality crystal was obtained. The crystal of the complex with compound **6** showed superior diffraction to that with compound **5**, and the crystal structure was solved at 1.64 Å resolution (R factor = 21.6%, R_{free} = 24.9%) and was identified as belonging to space group $P2_1$. Although the space group of the crystal of 17β-HSD5 complexed with compound **6** differs from that with compound **5**, no significant differences were noted in crystal packing. We therefore consider this crystal to belong to crystal form III, which is the same as the structure with compound **5** bound.

Compound **6** binds to the oxyanion site in the same manner as compound **5** and forms hydrogen bonds to Tyr55 (2.96 Å), His117 (2.85 Å) and the nicotinamide of $NADP^+$ (2.74 Å) (Fig. 7*b*). The hydroxyethyl group enters into the SP3 pocket and the hydroxyl group forms hydrogen bonds to the phosphate moiety of $NADP^+$ (2.67 Å) and the main-chain NH of Gln222 (2.57 Å). The hydroxyl group also interacts with the main-chain NH of Asp224 *via* a hydrogen bond to a water molecule. In PDB entry 1s1p, a water molecule is placed at the position of the hydroxyl group and forms similar hydrogen bonds, thus mimicking the water molecule. Loop C exhibits induced-fit conformational changes upon the binding of compound **6**. The main chain of loop C is rotated at Asp309, and a hydrogen bond is formed between the main-chain O atom of Asn307 and the main-chain NH of Ser310. The side chain of Phe311 is positioned on the indole ring of compound **6** and forms van der Waals and weak CH–π interactions with the indole ring. Consequently, Phe311 forms a hydrophobic

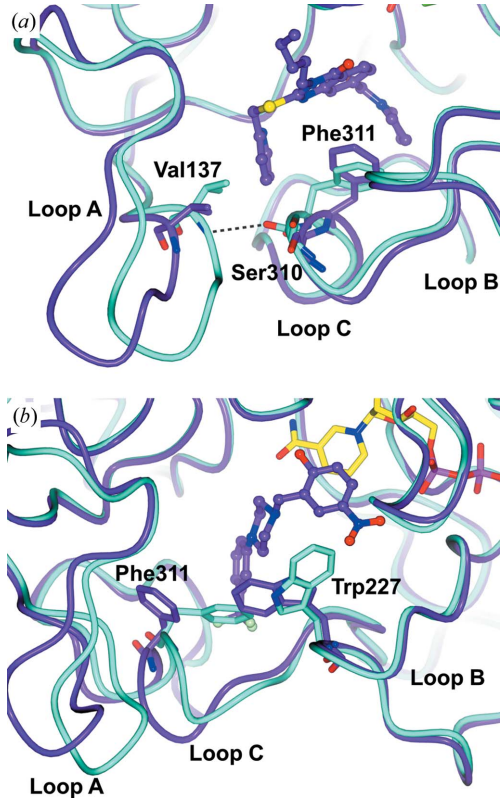

Figure 6
Structural changes of loops A, B and C upon binding inhibitor. Cyan indicates the protein structure of acetate-bound 17β-HSD5 (PDB entry 1s1p). The yellow stick model indicates $NADP^+$. (*a*) Purple indicates the protein structure of compound **1**-bound 17β-HSD5. The purple ball-and-stick model indicates compound **1**. (*b*) Purple indicates the protein structure of compound **4**-bound 17β-HSD5. The purple ball-and-stick model indicates compound **4**.

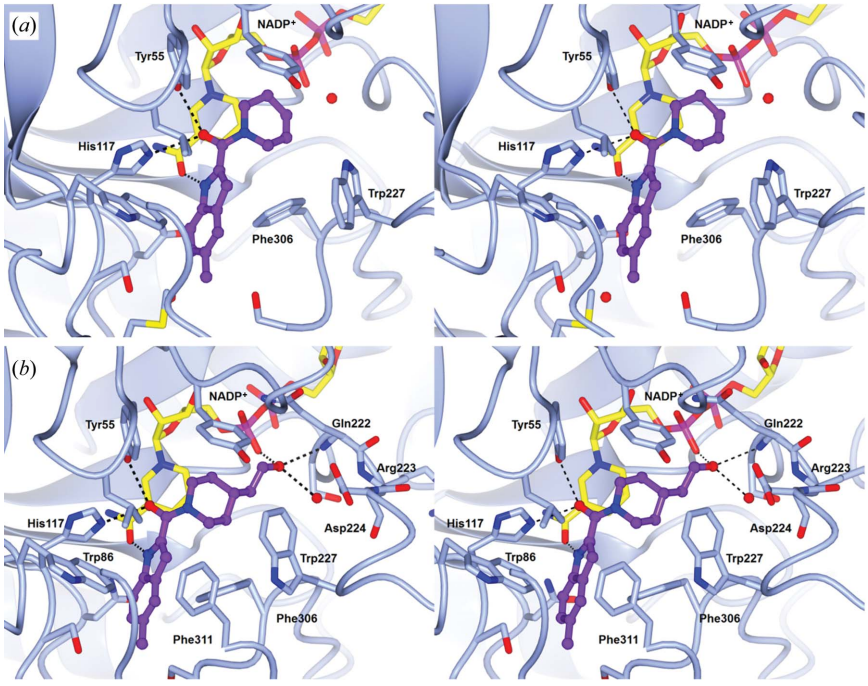

Figure 7
Stereo representations of crystal structures of inhibitor-bound 17β-HSD5. Purple ball-and-stick models indicate compounds **5** (*a*) and **6** (*b*). The yellow stick model indicates NADP$^+$. Red balls indicate water molecules.

tunnel surrounding the indole ring with Trp86 and Phe306, which also interact with the indole ring in the same manner as observed in the structure with compound **5** bound. In summary, the potent inhibitory activity of compound **6** is caused by the hydrogen-bonding network of the hydroxyethyl group in the SP3 pocket and the interaction of the indole ring in the newly formed hydrophobic tunnel.

Compound **6** was further optimized by Astellas Pharma and the orally bioavailable inhibitor ASP9521 was synthesized (Loriot *et al.*, 2014; Kikuchi *et al.*, 2014). Details of the optimization will be described elsewhere.

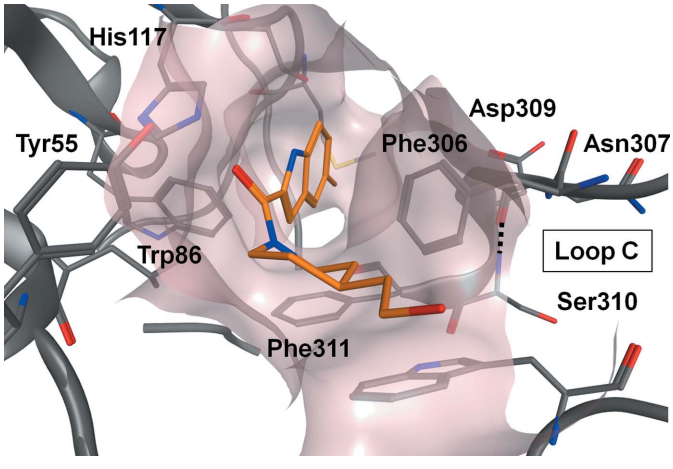

Figure 8
The hydrophobic tunnel generated by induced fit with compound **6**. The orange stick model indicates compound **6**. The grey ribbon model and stick model indicates the protein structure. Light brown indicates the protein surface around compound **6**. The dashed lines indicates hydrogen bonds in the protein.

3.7. New crystal forms

At present, there are 30 crystal structures of 17β-HSD5 in the PDB. 21 of these structures belong to the same crystal form as PDB entry 1s1p (crystal form I). In this study, we identified the new crystal forms II and III. In crystal form I, the residues Asn307, Ser308, Asp309, Ser313 and Pro315 in loop C are involved in interactions with crystallographic symmetry-related molecules (Fig. 9*a*). The side-chain and main-chain atoms of these residues make nine hydrogen bonds to symmetry-related molecules. This strong hydrogen-bond network of loop C is apparently required to generate crystal form I. Thus, cocrystallization with compounds **4**, **5** or **6** was unable to generate crystal form I because these compounds drastically change the conformation of loop C. In contrast, in loop C observed in crystal form II only Pro315 is close to the symmetry-related molecule and forms van der Waals interactions (Fig. 9*b*). A major portion of loop C is not involved in interaction with symmetry-related molecules; thus, crystal form II is suitable for the analysis of complex structures of ligands that change the conformation of the loop C drastically, such as compound **4**. Compounds **5** and **6** not only change the conformation of loop C but also disorder at least ten residues at the C-terminal end, including Pro315. Therefore, cocrystallization with compounds **5** or **6** was unable to generate crystal forms I or II.

3.8. Structural changes in loop C

Based on the structures with compounds **4**, **5** and **6**, we found that loop C, particularly residues Phe306–Phe311, undergoes induced-fit conformational changes upon binding. We analysed previously reported 17β-HSD5 structures and our structures, focusing on these amino-acid residues. Fig. 10(*a*) shows the r.m.s.d. values for all atoms or main-chain atoms from Phe306 to Phe311 against PDB entry 1s1p. For the previously reported structures, the patterns of structural changes can be classified into two groups. For PDB entries 1s2a (Lovering *et al.*, 2004), 3r8h, 3ug8 and 3ugr (Flanagan *et al.*, 2012), all atoms from Phe306 to Phe311 exhibit high r.m.s.d. values, whereas the main-chain atoms do not. In these structures, the side chains of Phe306 and Phe311 are flipped and apparently contribute to the high r.m.s.d. values and the similarity in structure between the main-chain atoms and PDB entry 1s1p. For PDB entries 1ry0, 1ry8 (Komoto *et al.*, 2004) and 2f38 (Komoto *et al.*, 2006), not only all atoms but also the main-chain atoms show high r.m.s.d. values. In these structures, the side chains of Phe306 and Phe311 were flipped, as in

PDB entries 1s2a, 3r8h, 3ug8 and 3ugr. In addition, rearrangement of the main-chain atoms is also observed. The structures of the main-chain atoms are similar to each other in these three structures (the r.m.s.d. values range from 0.40 to 0.69 Å). In contrast, 17β-HSD5 complexed with compound **6** exhibits higher r.m.s.d. values of main-chain atoms against PDB entry 1s1p compared with PDB entries 1ry0, 1ry8 and 2f38. To our knowledge, the main-chain conformation of residues Phe306–Phe311 in the compound **6**-bound structure differs from all previously reported structures (the r.m.s.d. values range from 2.82 to 4.04 Å) owing to differences in the mechanism of the structural changes. For PDB entries 1ry0, 1ry8 and 2f38, the ligands bind deeply into the SP1 pocket, flip the side chain of Phe311 and extend the SP1 pocket *via* movement of residues, including main-chain atoms. In contrast, compound **6** does not bind deeply into the SP1 pocket, instead binding in the SP3 pocket. The side chains of Phe306 and Phe311 move closer to the indole ring of compound **6**. The main-chain atoms also move towards the inside of the pocket and make the pocket smaller. Compound **6** effectively binds to this small pocket and exhibits potent inhibitory activity despite its low molecular mass (286.37 Da).

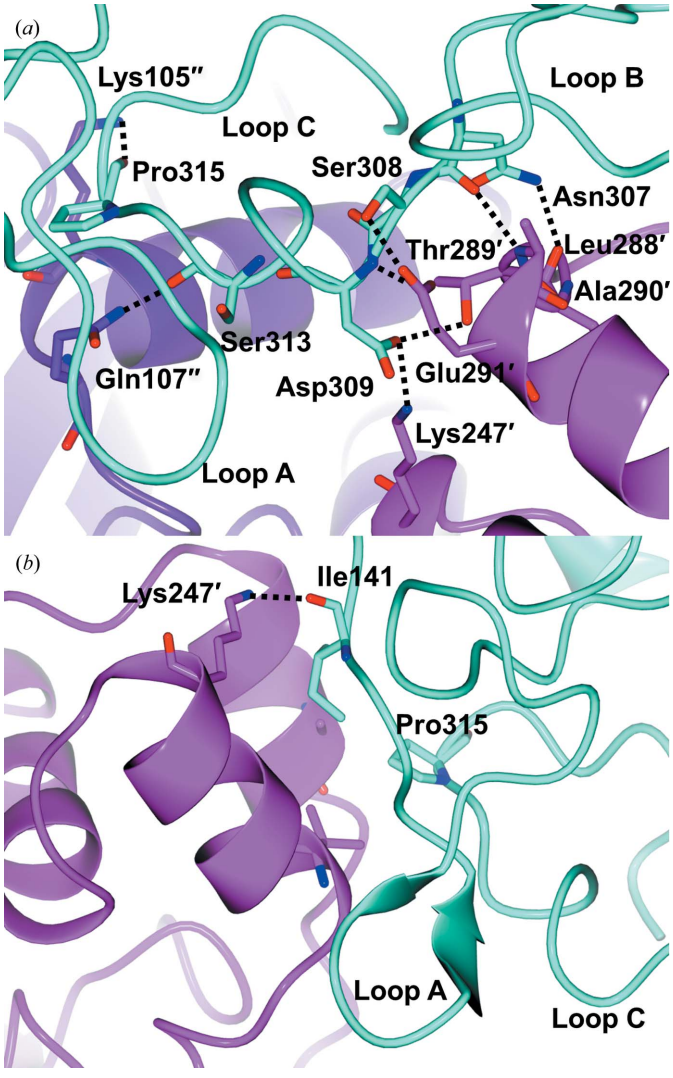

Figure 9
Interactions between loops A–C and crystallographic symmetry-related molecules observed in crystal forms I (*a*) (PDB entry 1s1p) and II (*b*) (compound **4**-bound form). Cyan indicates loops A–C. Crystallographic symmetry-related molecules are indicated in magenta and purple. Hydrogen bonds are depicted as dashed lines.

4. Conclusion

We solved crystal structures of 17β-HSD5 bound to structurally diverse inhibitors. These structures identified novel

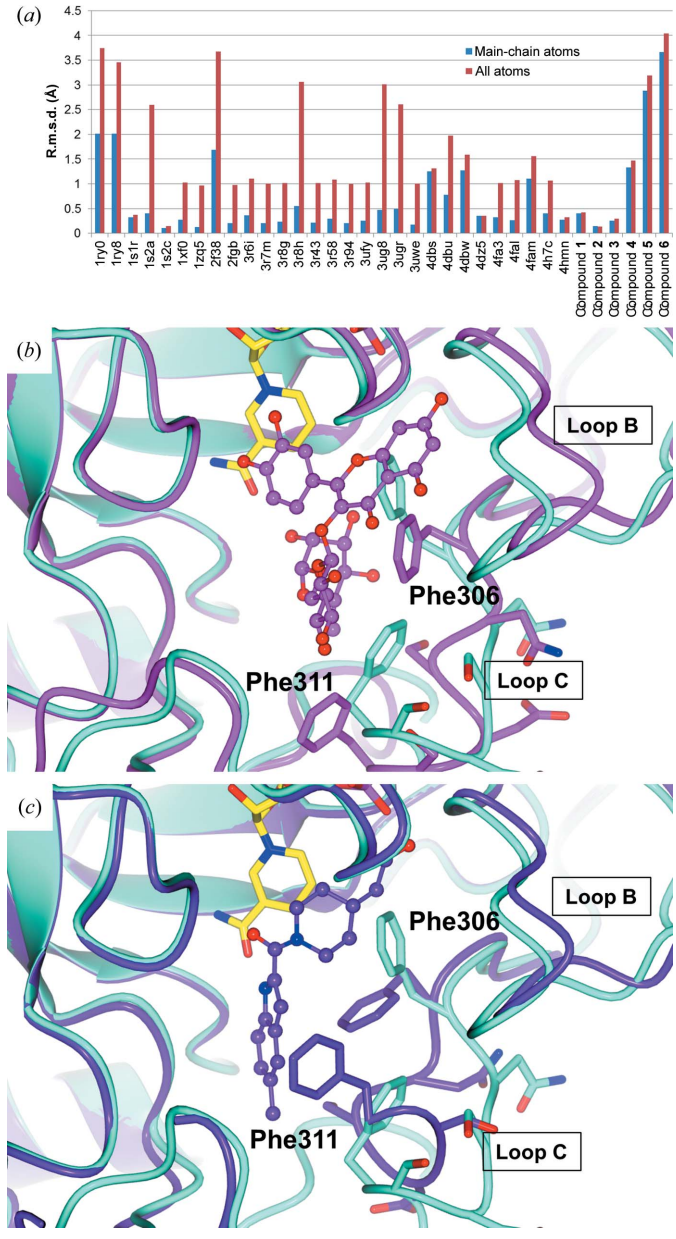

Figure 10
(*a*) R.m.s.d. values of residues Phe306–Phe311 against PDB entry 1s1p. (*b*, *c*) PDB entry 1ry8 (*b*) and the compound **6**-bound structure (*c*) superposed on PDB entry 1s1p. Magenta indicates PDB entry 1ry8, cyan PDB entry 1s1p and purple the compound **6**-bound structure. Ball-and-stick models indicate the inhibitor compounds. Stick models represent side-chain atoms from Phe306 to Phe311. The yellow stick model indicates $NADP^+$.

scaffolds that bind to the oxyanion site. In particular, in compound **3** the N atoms of the pyrazole ring bound to the oxyanion site. To our knowledge, this is the first example of the binding of atoms other than oxygen to the oxyanion site. This finding may lead to the generation of novel 17β-HSD5 inhibitors with different physicochemical properties from known 17β-HSD5 inhibitors which have a carboxylic acid or a carbonyl O atom. We also observed conformational changes in loop C and the C-terminal end of 17β-HSD5 upon binding to an inhibitor. These changes generated the new crystal forms II and III. In crystal form III, we observed a new conformation of the loop C that is fairly distinct from that in previously reported 17β-HSD5 structures and revealed the mechanism of its potent inhibition by compound **6**. To reveal the true binding modes of inhibitors, cocrystallization with inhibitors, including exploration of new crystallization conditions, should possibly precede soaking methods, particularly for catalytic pockets consisting of potentially flexible loops. Our findings might facilitate the structure-based drug design of 17β-HSD5 inhibitors and drug development for anti-CRPC therapy.

Acknowledgements

We thank Dr Kentaro Enjo for providing enzyme-assay data and the beamline staff at Photon Factory, KEK, Japan for assisting with data collection.

References

Adeniji, A. O., Chen, M. & Penning, T. M. (2013). *J. Steroid Biochem. Mol. Biol.* **137**, 136–149.
Byrns, M. C., Jin, Y. & Penning, T. M. (2011). *J. Steroid Biochem. Mol. Biol.* **125**, 95–104.
Byrns, M. C., Steckelbroeck, S. & Penning, T. M. (2008). *Biochem. Pharmacol.* **75**, 484–493.
Chavas, L. M. G., Matsugaki, N., Yamada, Y., Hiraki, M., Igarashi, N., Suzuki, M. & Wakatsuki, S. (2012). *J. Synchrotron Rad.* **19**, 450–454.
Chen, M., Adeniji, A. O., Twenter, B. M., Winkler, J. D., Christianson, D. W. & Penning, T. M. (2012). *Bioorg. Med. Chem. Lett.* **22**, 3492–3497.
Emsley, P. & Cowtan, K. (2004). *Acta Cryst.* D**60**, 2126–2132.
Flanagan, J. U., Atwell, G. J., Heinrich, D. M., Brooke, D. G., Silva, S., Rigoreau, L. J., Trivier, E., Turnbull, A. P., Raynham, T., Jamieson, S. M. & Denny, W. A. (2014). *Bioorg. Med. Chem.* **22**, 967–977.
Flanagan, J. U., Yosaatmadja, Y., Teague, R. M., Chai, M. Z. L., Turnbull, A. P. & Squire, C. J. (2012). *PLoS One*, **7**, e43965.
Heinrich, D. M., Flanagan, J. U., Jamieson, S. M., Silva, S., Rigoreau, L. J., Trivier, E., Raynham, T., Turnbull, A. P. & Denny, W. A. (2013). *Eur. J. Med. Chem.* **62**, 738–744.
Jackson, V. J., Yosaatmadja, Y., Flanagan, J. U. & Squire, C. J. (2012). *Acta Cryst.* F**68**, 409–413.
Jamieson, S. M. *et al.* (2012). *J. Med. Chem.* **55**, 7746–7758.
Kikuchi, A., Furutani, T., Azami, H., Watanabe, K., Niimi, T., Kamiyama, Y., Kuromitsu, S., Baskin-Bey, E., Heeringa, M., Ouatas, T. & Enjo, K. (2014). *Invest. New Drugs*, **32**, 860–870.
Komoto, J., Yamada, T., Watanabe, K. & Takusagawa, F. (2004). *Biochemistry*, **43**, 2188–2198.
Komoto, J., Yamada, T., Watanabe, K., Woodward, D. F. & Takusagawa, F. (2006). *Biochemistry*, **45**, 1987–1996.
Labrie, F. (2011). *Nature Rev. Urol.* **8**, 73–85.
Liedtke, A. J., Adeniji, A. O., Chen, M., Byrns, M. C., Jin, Y., Christianson, D. W., Marnett, L. J. & Penning, T. M. (2013). *J. Med. Chem.* **56**, 2429–2446.
Loriot, Y., Fizazi, K., Jones, R. J., Van den Brande, J., Molife, R. L., Omlin, A., James, N. D., Baskin-Bey, E., Heeringa, M., Baron, B., Holtkamp, G. M., Ouatas, T. & De Bono, J. S. (2014). *Invest. New Drugs*, **32**, 995–1004.
Lovering, A. L., Ride, J. P., Bunce, C. M., Desmond, J. C., Cummings, S. M. & White, S. A. (2004). *Cancer Res.* **64**, 1802–1810.
Murshudov, G. N., Skubák, P., Lebedev, A. A., Pannu, N. S., Steiner, R. A., Nicholls, R. A., Winn, M. D., Long, F. & Vagin, A. A. (2011). *Acta Cryst.* D**67**, 355–367.
Otwinowski, Z. & Minor, W. (1997). *Methods Enzymol.* **276**, 307–326.
Penning, T. M., Burczynski, M. E., Jez, J. M., Hung, C.-F., Lin, H.-K., Ma, H., Moore, M., Palackal, N. & Ratnam, K. (2000). *Biochem. J.* **351**, 67–77.
Qiu, W., Zhou, M., Labrie, F. & Lin, S.-X. (2004). *Mol. Endocrinol.* **18**, 1798–1807.
Qiu, W., Zhou, M., Mazumdar, M., Azzi, A., Ghanmi, D., Luu-The, V., Labrie, F. & Lin, S.-X. (2007). *J. Biol. Chem.* **282**, 8368–8379.
Vagin, A. & Teplyakov, A. (2010). *Acta Cryst.* D**66**, 22–25.
Watanabe, K., Kakefuda, A., Yasuda, M., Enjo, K., Kikuchi, A., Furutani, T., Naritomi, Y., Otsuka, Y., Okada, M. & Ohta, M. (2013). *Bioorg. Med. Chem.* **21**, 5261–5270.